Viewing angle-enhanced integral imaging system using three lens arrays

Wei Xie (谢 伟), Yazhou Wang (王亚洲), Huan Deng (邓 欢), and Qionghua Wang (王琼华)*

School of Electronics and Information Engineering, Sichuan University, Chengdu 610065, China

**Corresponding author: qhwang@scu.edu.cn*

Received Augnst 2, 2013; accepted October 17, 2013; posted online December 5, 2013

We propose an integral imaging system that uses three lens arrays, including two convex lens arrays and a concave lens array. Compared with the conventional integral imaging system, the proposed system can remarkably enhance the viewing angle. The maximum viewing angle can be enlarged to 48°, which is 4.8 times wider than that of the conventional system. The principle of the proposed system is elucidated, and the experimental results are presented in this letter.

OCIS codes: 110.6880, 080.2740, 120.4640.
doi: 10.3788/COL201412.011101.

Three-dimensional (3D) imaging and visualization techniques have generated significant interest[1−6]. Integral imaging, which was first proposed by Lippmann in 1908[7], has attracted the most attention among 3D imaging techniques. Integral imaging is considered as one of the most practical 3D display techniques because it does not require special glasses and provides a continuous viewing point within the viewing angle. Moreover, this technique provides both horizontal and vertical parallaxes and displays real-time 3D dynamic images. Compared with holography, this technique does not require a coherent light source and displays images with full natural colors. In spite of these advantages, the technique has several problems, such as a narrow viewing angle, a limited depth of field, and low resolution. All these disadvantages should be resolved to deploy the technique successfully on a commercial level. The limitation on viewing angle is considered as the primary disadvantage of integral imaging. The viewing angle of conventional integral imaging is typically less than 10°, which seriously restraints the practical application of this technique[8].

In conventional integral imaging, the limitation on viewing angle is primarily attributed to the small size of the lenses in the lens array[8]. This limitation is also associated with the flipping of elemental images that correspond to neighboring lenses, that is, the viewing angle is limited by the size of the elemental image and the focal length of the lens. Numerous methods have been proposed to overcome this disadvantage such as volume holographic memory, two elemental image masks, electrically movable pinhole array, moving lens let arrays, viewer tracking system, and refraction index medium[9−21]. We have also proposed a system to increase the viewing angle by using two lens arrays[22].

In this letter, we propose a system to expand the viewing angle of integral imaging. The configuration of the proposed integral imaging system is shown in Fig. 1. The system is composed of a two-dimensional (2D) display screen with a liquid crystal display, two convex lens arrays, one concave lens array, and two barrier arrays. The 2D display screen is used to display the elemental images, and the two barrier arrays are used to eliminate crosstalk between adjacent lenses from the horizontal and vertical directions. The two convex lens arrays are used to provide amplified virtual elemental images to the concave lens array. A 3D image is reconstructed in front of the concave lens array.

In integral imaging, the maximum viewing angle is restricted to the region wherein the integrated image is continuously observed without flipping. The pitch of the lens is p, and the gap between the lens array and the elemental image is g. When the elemental lens is in the air, the incident angle is equivalent to the viewing angle Ω_0. Thus, the maximum viewing angle Ω_0 for a single lens is given by $\Omega_0 = 2\arctan(\frac{p}{2g})$. In fact, the maximum viewing angle θ_0 for the entire system is less than Ω_0. m is assumed as the dimension of the lens array, and l is the distance between the viewer and the lens array. To observe the image continuously without flipping, the viewer must stay in the viewing zone. Thus, a minimum viewing distance l_{c0} exists. Based on the geometric relationship, θ_0 and l_{c0} are given as[23]

$$\theta_0 = 2\arctan\Big(\frac{pl - pg(m-1)}{2gl}\Big), \tag{1}$$

$$l_{c0} = (m-1)g. \tag{2}$$

The reconstruction of the proposed system, in which only one lens in each array is considered, is shown in

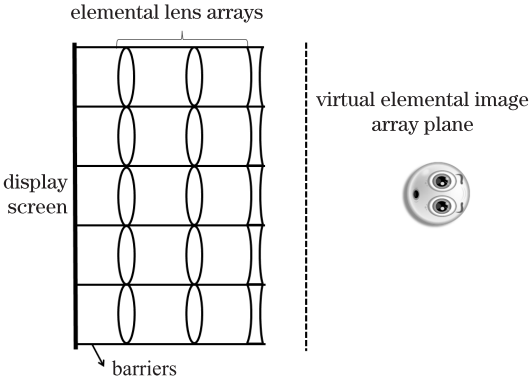

Fig. 1. Schematic diagram of the proposed integral imaging system.

Fig. 2. The two convex lenses and the concave lens are labeled as lenses 1, 2, and 3, respectively. The elemental image on the 2D display screen first passes through lens 1 and forms an amplified virtual elemental image 1 at the back plane of the screen. The light rays then pass through lens 2 and form a virtual elemental image 2, which is located before the focal plane of lens 3. Virtual elemental image 2 can be considered as the elemental image of lens 3. The pitch of virtual elemental image 2 is denoted as p', and $p' = Vp$, where V is the product of the lateral magnification of the two convex lenses. As shown in Fig. 3, the maximum viewing angle Ω for a single lens in the proposed integral imaging system is given by $\Omega = 2\arctan(\frac{Vp}{2g})$. The maximum viewing angle θ and the minimum viewing distance l_0 are given by

$$\theta = 2\arctan\Big(\frac{pVl - pg(m-1)}{2gl}\Big), \tag{3}$$

$$l_0 = \frac{(m-1)g}{V}, \tag{4}$$

where p and l have the same definitions as those in conventional integral imaging, and g is the gap between the concave lens array and virtual elemental image 2.

Comparing Eqs. (1) and (3) under fixed p and g, if $V > 1$, then each virtual elemental image will overlap with adjacent ones and the viewing angle will expand.The viewing angle becomes large with increasing V. As shown in Fig. 2, the focal lengths of lenses 1 and 2 are f_1 and f_2, respectively. The lateral magnifications of lenses 1 and 2 are V_1 and V_2, respectively. $V_1 \cdot p$ and $V \cdot p$ are the pitches of virtual elemental images 1 and 2, respectively. H_2 and H_2' are the principal planes of lens 2. L_1 is the distance between virtual elemental image 1 and H_2. L_2 is the distance between H_2' and the right edge of lens 3. D_1 and D_2 are the thicknesses of lenses 1 and 2, respectively. d_1 and d_2 are the pitches between the two principal planes of Lenses 1 and 2, respectively. For lens 2, the value of V_2 can be described as $V_2 = \frac{L_2+g'-f_2}{f_2}$; thus, $V = V_1 \cdot V_2$ is proportional to L_2 when V_1 is fixed. However, the value of L_2 is limited by the structure of the display panel. As shown in Fig. 2, the lights coming from A and B are partly absorbed by the optical barrier. To prevent the lights coming from the edge of the original elemental image from being absorbed mostly by the optical barrier, we acquire the distance between the original elemental images and assume that H_2 is equal to L_2. Using the lens law and geometric relation, we obtain

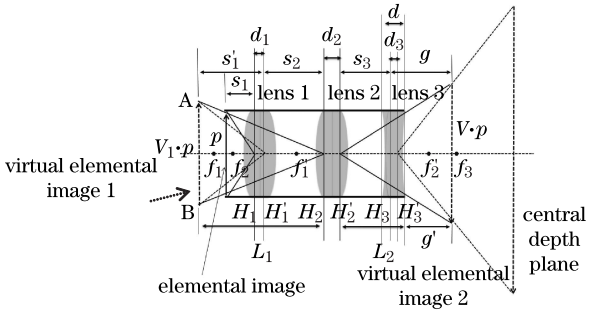

Fig. 2. (Color online) Optical path diagram and the parameters of the proposed integral imaging system.

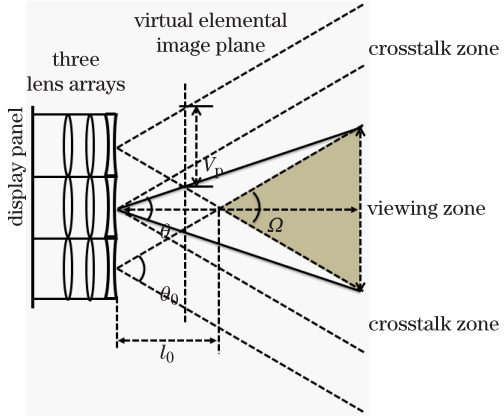

Fig. 3. (Color online) Maximum viewing angles of the conventional integral imaging system.

$$\frac{V_1 \cdot p}{L_1} = \frac{p}{L_2}, \tag{5}$$

$$\frac{1}{L_1} + \frac{1}{L_2 + g'} = \frac{1}{f_2}, \tag{6}$$

$$g' = g - \frac{d}{2} - \frac{d_3}{2}, \tag{7}$$

where d and d_1 are the edge thickness and the gap between the two principal planes of lens 3, respectively. g' is the distance between virtual elemental image 2 and the right edge of lens 3. When V_1 is given, L_1 and L_2 can be calculated as

$$L_1 = \frac{(1+V_1)f_2 - gV_1 + \sqrt{(g-f_2)^2V_1^2 + 2V_1f_2(g+f_2) + f_2^2}}{2}, \tag{8}$$

$$L_2 = \frac{L_1}{V_1}. \tag{9}$$

The distance between the original elemental images and H_1 is denoted as s_1, that between H_1' and H_2 as s_2, and that between H_2' and H_3 as s_3. These parameters are expressed as

$$s_1 = \frac{f_1V_1 - f_1}{V_1}, \tag{10}$$

$$s_2 = L_1 - V_1s_1, \tag{11}$$

$$s_3 = L_2 - \frac{d}{2} - \frac{d_3}{2}, \tag{12}$$

$$V = \frac{V_1f_2}{L_1 - f_2}. \tag{13}$$

In the proposed system, s_2 is alterable and has a minimum value. The two convex lens arrays adjoin each other. s_1 is less than f_1. To decrease aberration, s_1 should not be too small. Thus, we set $f_1 > s_1 \geqslant 3.5$. If

d, d_3, and g remain constant, then the values of f_1, f_2, s_1, s_2, and s_3 can be adjusted to find the largest V that satisfies the following limitation conditions: $f_1 > s_1 \geqslant 3.5$ and $s_2 \geqslant \frac{1}{2}(D_1 - d_1 + D_2 - d_2)$. The focal length of lens 3 is set as 3.5 mm, and the value of g is 3.395 mm. By using Eqs. (5)–(13) and the iterative computations, we find that the suitable V is 2.063 and that the focal lengths of lenses 1 and 2 are 4.5 and 5.2 mm, respectively. If p = 2 mm, m=66, and l=400 mm, then the calculated maximum viewing angles θ and θ_0 are 48° and 10°, respectively. Hence, the viewing angle of the proposed method is 4.8 times wider than that of conventional integral imaging.

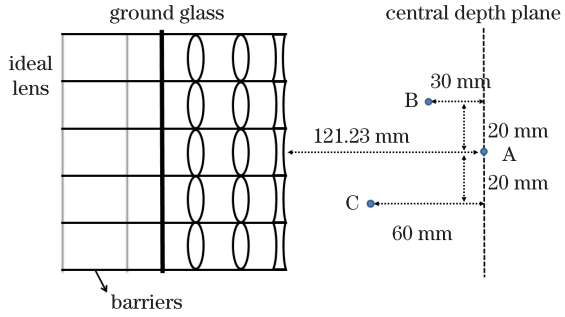

Fig. 4. Sketch map of the main geometry of the proposed system.

Table 1. Main Parameters Used in ASAP Simulation for the Proposed System

Parameters	Values (mm)
Focal Length of Lens 1 (f_1)	4.5
Focal Length of Lens 2 (f_2)	5.2
Focal Length of Lens 3 (f_3)	3.5
Interval between the Ground Glass and Lens 1 (s_1)	3.704
Interval between Lenses 1 and 2 (s_2)	0.446
Interval between Lenses 2 and 3 (s_3)	3.465
Interval between the Virtual Elemental Image and Lens 3 (g)	3.395
Viewing Distance (l)	400
Position of Light Source A	(0, 0, –129.96)
Position of Light Source B	(–20, –20, –91.23)
Position of Light Source C	(20, 20, –61.23)

Table 2. Main Parameters Used in ASAP Simulation for Conventional Integral Imaging

Parameters	Values (mm)
Focal Length of the Elemental Lens (f)	3.5
Interval between the Ground Glass and the Lens (s)	3.607
Interval between the Elemental Image and the Elemental Lens (g)	3.395
Viewing Distance (l)	400
Position of Light Source A	(0, 0, –238.26)
Position of light source B	(–20, –20, –123)
Position of light source C	(15, 15, –183)

We use the advanced systems analysis program (ASAP) to simulate the proposed and conventional systems. To compare the two systems under similar conditions, the focal length of the conventional lens is equal to that of lens 3 in the proposed system. The two systems should also have the same viewing distance and the same parameters for the lens array. We use the equivalent ideal lens, instead of lenses 1, 2, and 3, in the pickup process to obtain high-quality elemental images. The elemental image generated by the ideal lens is recorded by a ground glass and is scattered on the back of the glass to provide the elemental image for reconstruction. During reconstruction, the central thickness values of lenses 1 and 2 are both 0.6 mm, and the edge and central thickness values of lens 3 are 0.6 and 0.1 mm, respectively. The barriers are rectangular plates with a width of $p \cdot m$ cm, and the length is equal to the distance from the edge of the concave lens to the border of the corresponding ideal lens. The sketch map of the main geometry of the proposed system in ASAP simulation is shown in Fig. 4. We choose three dot light sources distributed around the object central depth plane. The dimension of the lens array is 72×72, whereas that of the recorded elemental image is 66×66. In the simulation, the three lenses have the same refractive index of 1.55. The viewing distance is 400 mm. From the view point at the center of the viewing angle, we set two camera arrays in horizontal and vertical directions in the plane parallel to the display. Apart from the center, the cameras are rotated to certain degrees to enable their optical axes to cross the central point of the concave lens array. The main parameters used in the ASAP simulation of the two systems are listed in Tables 1 and 2, respectively.

To compare the two systems clearly, both the horizontal and vertical viewing angles are considered. The images captured by the cameras from different viewing directions in the proposed system are shown in Figs. 5(a)-(j). Meanwhile, the images captured in the conventional system are presented in Figs. 6(a)-(j). In Fig. 5, the images of the three light sources within the viewing angle ±24° are presented clearly. When the viewing angle exceeds ±24°, the images become blurred. Thus, the effective viewing angle is 48°, which is consistent with the calculated results. Within the effective viewing angle range, the images are all observed clearly in the four directions, that is, left, right, up, and down. For the conventional system, the calculated viewing angle is 10°.

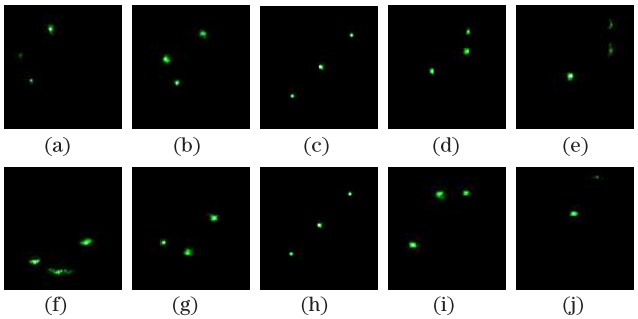

Fig. 5. (Color online) Integral images captured from different viewing angles along the horizontal and vertical directions of the proposed scheme: (a) left 25 °, (b) left 24 °, (c) 0 °, (d) right 24 °, (e) right 25 °, (f) down 25 °, (g) down 24 °, (h) 0 °, (i) up 24 °, and (j) up 25 °.

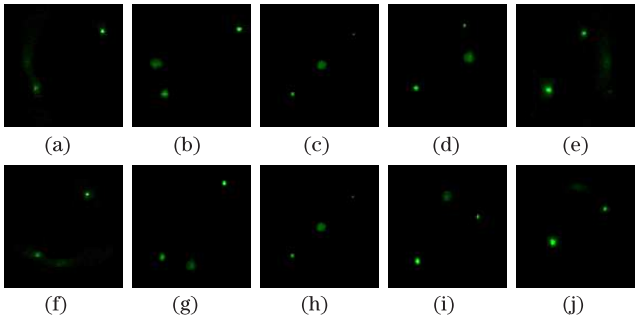

Fig. 6. (Color online) Integral images captured from different viewing angles along the horizontal and vertical directions of the conventional integral image: (a) left 6 °, (b) left 5 °, (c) 0 °, (d) right 5 °, (e) right 6 °, (f) down 6 °, (g) down 5 °, (h) 0 °, (i) up 5 °, and (j) up 6 °.

Thus, the viewing angle of the proposed system is approximately 4.8 times wider than that of the conventional system. In Ref. [22], our group used two elemental lens arrays to enhance the viewing angle. The maximum viewing angle can be enlarged to 32°. Therefore, the proposed system is also significantly better than the two-elemental lens array system.

In conclusion, we propose an integral imaging system that uses three lens arrays. The proposed system could remarkably enhance the viewing angle compared with the conventional system. Through ASAP simulation, we demonstrate that the viewing angle can be expanded to 48°, which is 4.8 times wider than that of the conventional integral image. Our system can be used to realize a 3D display that is free from the limitation of the viewing angle.

This work was supported by the National "973" Program of China (No.2013CB328802), the National Natural Science Foundation of China (Nos. 61225022 and 61036008), and the National "863" Program of China (Nos. 2012AA011901 and 2012AA03A301).

References

1. Q. Wang, H. Deng, T. Jiao, D. Li, and F. Wang, Chin. Opt. Lett. **8,** 512 (2010).
2. H. Deng, Q. Wang, D. Li, C. Luo, and C. Ji, Chin. Opt. Lett. **11,** 041101 (2013)
3. Q. Wang, Y. Tao, W. Zhao, and D. Li, Chin. Opt. Lett. **8,** 373 (2010).
4. Y. Wang, H. Deng, C. Luo, and Q. Wang, Chin. Opt. Lett. **11,** 061101 (2013).
5. B. Lee, S.-Y. Jung, S.-W. Min, and J.-H. Park, Opt. Lett. **26,** 1481(2001).
6. S.-H. Hong, J.-S. Jang, and B. Javidi, Opt. Express **12,** 483 (2004).
7. G. Lippmann, Comptes-Rendus Acad. Sci. **146,** 446 (1908).
8. Y. Kim, K. Hong, and B. Lee, 3D Res. **01,** 17 (2010).
9. S. Shin and B. Javidi, Appl. Opt. **41,** 5562 (2002).
10. Y. Kim, J. Kim, J.-M. Kang, J.-H. Jung, H. Choi, and B. Lee, Opt. Express **15,** 18253 (2007).
11. H. Choi, S.-W. Cho, J. Kim, and B. Lee, Opt. Express **14,** 5183 (2006).
12. H. Choi, J.-H. Park, J. Kim, S.-W. Cho, and B. Lee, Opt. Express **13,** 8424 (2005).
13. C.-G. Luo, C.-C. Ji, F.-N. Wang, Y.-Z. Wang, and Q.-H. Wang, J. Display Technol. **8,** 634 (2012).
14. S. Jung, J.-H. Park, H. Choi, and B. Lee, Opt. Express **11,** 1346 (2003).
15. R. Martínez-Cuenca, H. Navarro, G. Saavedra, B. Javidi, and M. Martínez-Corral, Opt. Express **15,** 16255 (2007).
16. J.-S. Jang and B. Javidi, Appl. Opt. **42,** 1996 (2003).
17. G. Park, J.-H. Jung, K. Hong, Y. Kim, Y.-H. Kim, S.-W. Min, and B. Lee, Opt. Express **17,** 17895 (2009).
18. G. Baasantseren, J.-H. Park, K.-C. Kwon, and N. Kim, Opt. Express **17,** 14405 (2009).
19. Y. Kim, J.-H. Park, S.-W. Min, S. Jung, H. Choi, and B. Lee, Appl. Opt. **44,** 546 (2005).
20. S. Jung, J.-H. Park, H. Choi, and B. Lee, Appl. Opt. **42,** 2513 (2003).
21. J.-Y. Jang, H.-S. Lee, S. Cha, and S.-H. Shin, Appl. Opt. **50,** 71 (2011).
22. Y.-Z. Wang, D.-H. Li, C.-G. Luo, and Q.-H. Wang, J. Soc. Inf. Display **21,** 289 (2013).
23. H. Deng, Q. H. Wang, L. Li, and D. H. Li, J. Soc. Inf. Display **19,** 679 (2011).